Electronic Supplementary Material (ESI) for Environmental Science: Processes & Impacts.
This journal is © The Royal Society of Chemistry 2023

SUPPLEMENTAL MATERIAL FOR

Chemical Characterization of Microplastic Particles Formed in Airborne Waste Discharged from Sewer Pipe Repairs

Brianna N. Peterson,[1] A.C. Morales,[1] J.M. Tomlin,[1] C.G.W. Gorman,[1] P.E. Christ,[1] S.A.L. Sharpe,[1] S.M. Huston,[1] F.A. Rivera-Adorno,[1] B.T. O'Callahan,[3] M. Fraund,[4] Y. Noh,[5] P. Pahari,[5] A.J. Whelton,[5,6] P.Z. El-Khoury,[7] R.C. Moffet,[4] A. Zelenyuk,[8] A. Laskin.* [1,2]

[1]Department of Chemistry, [2]Department of Earth, Atmospheric and Planetary Sciences, Purdue University, West Lafayette, IN, USA

[5]Environmental Molecular Sciences Laboratory, [7]Physical Sciences Division, [8]Atmospheric Sciences and Global Change Division, Pacific Northwest National Laboratory, Richland, WA, USA

[4]Sonoma Technology, Inc., Petaluma, CA, USA

[5]Lyles School of Civil Engineering, [6]Department of Environmental and Ecological Engineering, Purdue University, West Lafayette, IN, USA

Table of Contents

Supplementary Note 1: Sample collection and preparation for analysis

Waste samples were collected from CIPP installations at construction sites in Sacramento, California.[1] These were X1 and X2 as identified in Morales et al., 2022.[2] Stainless steel air manifolds were set up at sampling sites to catch and condense the steam emission plume. Condensed samples were collected in Pyrex bottles and stored at -20 °C.[1] The styrene-based waste was collected at site using an isophthalic based polyester resin with 0.5% Trigonox® KSM and 1% di-(4-tert-butylcyclohexyl) peroxy decarbonate initiators.[1] The vinyl ester-based waste was collected at a site using EcoTek™ L040-TNVG-33 vinyl ester resin, but no disclosed initiators.[1]

Composites were cured in a custom built laboratory curing chamber as shown in Figure S1 placed inside a thermal oven within a fume hood.[3] Resin impregnated felt blocks were placed on a Teflon® release film and placed in the chamber, which was sealed for the duration of curing.[3] Curing was conducted under vacuum and resulted in a hard cured composite.

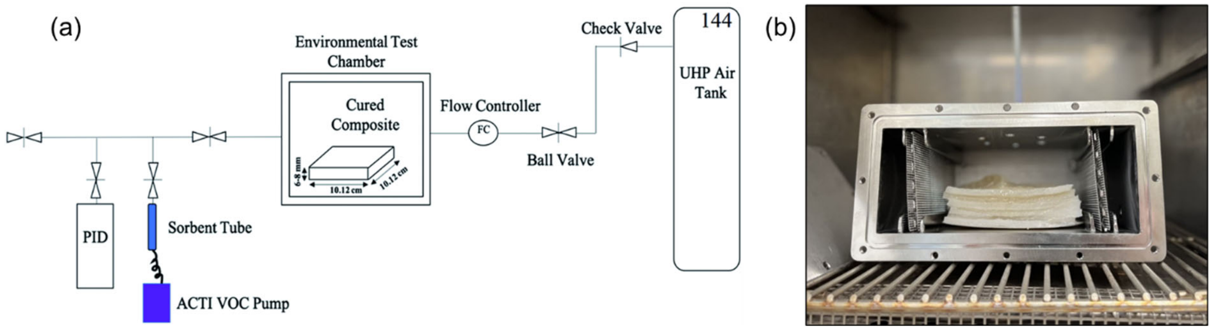

Figure S1. The experimental setup used to cure the composites in the laboratory setting. Panel (a) shows the schematic of the setup. Panel (b) displays a photograph of the test chamber, shown with a block of cured composite inside. Panel a is reproduced from Sendesi et al, 2020.[3] Copyright 2020, Royal Society of Chemistry.

Photographs of the uncured resin, cured composite, and discharged steam laden waste emitted at the installation site are displayed in Figure S2.

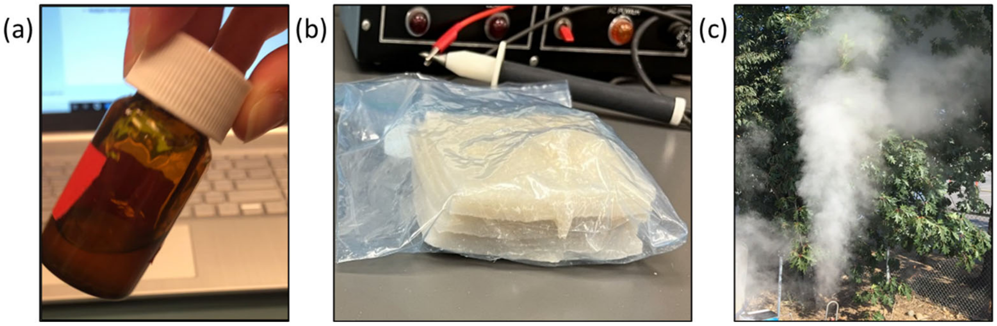

Figure S2. (a) Sample vial containing styrene-based resin, (b) pieces of cured composite that was powdered and suspended in ethanol, and (c) steam-laden waste released during CIPP installation that was condensed in cold traps at field sites.

Supplementary Note 2: Chemical imaging techniques used for single particle analysis.

SERS experiments were performed using a commercial Raman microscope (LabRAM, Horiba). Suspensions of the analyte were dropcast onto a Au film (50 nm thickness) prepared using a desktop sputter coater (target: Ted Pella Inc., 99.99%). Less than 5 mW of 785 nm laser light source was focused onto the microparticles with a 100x 0.9 NA objective. Spectra were acquired for 30-60s at ~1 cm^{-1} spectral resolution. The spectral range from 100 cm^{-1} to 3500 cm^{-1} was covered by combining 5 separate acquisitions of ~800 cm^{-1} at different grating positions.

STXM-NEXAFS was used to analyze individual particles of resin, composite, and waste composition. STXM-NEXAFS is a synchrotron-based X-ray microscopy technique that raster scans the sample through a monochromatic X-ray beam focused by a Fresnel zone plate. An order sorting aperture is used between the zone plate and analyte to decrease any higher-order diffracted light.[4] The order sorting aperture allows spectra of higher resolution to be obtained.[4] The X-ray beam is scanned through different energy levels to produce "stacks" which take a spectral image by measuring transmitted X-rays at 96 energies between 278 to 320 eV with 1 ms dwell time. Spectral "maps" are acquired by capturing images at four fundamental energy levels: 278 eV (carbon pre-edge), 285.4 eV (C=C), 288.5 eV (-COOH), and 320 eV (carbon post-edge). The spatial resolution of STXM-NEXAFS depends on the zone plate used to focus the X-ray beam.[4] Spot sizes of 25 nm are typically achieved and spot sizes down to 15 nm have been reported.

STXM-NEXAFS enables the acquisition of the spatially resolved information on chemical bonding and oxidation state of carbon within individual particles. When core-shell electrons absorb the soft X-rays utilized by STXMs, they undergo absorption as the electron is excited.[4] As the X-ray beam is scanned through the energy levels, characteristic peaks occur as carbon functionalities absorb at specific energies. Information about bond hybridization is also provided by the location and intensity of both the $1s \rightarrow \pi^*$ and $1s \rightarrow \sigma^*$ electronic transitions. sp^2 bonding is π-like, while sp^3 bonding will be more σ-like.[5]

STXM-NEXAFS detects the transmitted light through a sample. Beer's law is used to convert the measured transmitted light to optical density (OD_E), which is then plotted against X-ray energy to generate a spectrum for each particle.

$$OD_E = -\ln\left(\frac{I(E)}{I_0(E)}\right. = \mu\rho t$$

In this equation, $I_0(E)$ represents transmitted light in areas without particles, $I(E)$ represents transmitted light through regions of particles, μ is the mass absorption coefficient, ρ is the mass density, and t is the thickness of the sample.

For individual particle analysis, an established workflow through use of MATLAB scripts was used.[6–10] Briefly, components within a particle are classified into three categories based on defined thresholds. "Organic carbon" (OC) is defined as the difference in the OD of the carboxylic acid peak (288.5 eV) and the carbon pre-edge peak (278 eV) greater than zero. "sp^2-hybridized carbon" is defined as the proportion of the intensity of the C=C peak (285.4 eV) to the total carbon absorption (OD_{320eV}-OD_{278eV}) compared to a highly oriented pyrolytic graphite (HOPG) standard[11] as defined below:

$$\frac{OD_{285.4}^{Sample}}{OD_{320\,eV}^{Sample} - OD_{278\,eV}^{Sample}} : \frac{OD_{320eV}^{HOPG} - OD_{278\,eV}^{HOPG}}{OD_{285.4\,eV}^{HOPG}} > 0.35$$

"Inorganics" (IN) are defined as regions where the ratio of OD_{278eV} (carbon pre-edge) to OD_{320eV} (carbon post-edge) is greater than 0.5. These different components are then superimposed onto the particle to gain a spatially resolved picture of particle composition.

Supplementary Note 3: Real-time characterization of individual aerosolized particles.

The size (vacuum aerodynamic diameter, d_{va}) and mass spectra of individual particles were measured in real-time by the single particle mass spectrometer, miniSPLAT, which is described in detail elsewhere[12]. miniSPLAT uses an aerodynamic lens inlet to generate a narrow low divergence particle beam and transmit the particles into the vacuum chamber with high efficiency. Each particle exiting the lens acquires a velocity that is a narrow function of its d_{va}. Individual particles are then detected via light scattering at two optical stages placed 10.9 cm apart. The particle time-of-flight between the two stages allows the calculation of particle velocity and its d_{va}, with precision and accuracy better than 0.5%. Once a particle is detected in both optical stages, its time-of-flight is also used to generate the trigger for pulsed ablation/ionization excimer laser.[13] Individual particle mass spectra are then collected by a dual-polarity Z-configuration time-of-flight mass spectrometer (TOF-MS).

Supplementary Note 4: Molecular characterization of bulk samples.

The DART source operates by generating a corona discharge between a needle and a perforated disk electrode.[14] The corona discharge produces a mixture of ions, electrons, and excited gas atoms.[14] Charged particles are removed as the ions, electrons, and gas atoms pass through different metal grids within the source.[15] The grid at the end of the DART source prevents ion-ion and ion-electron recombination, provides a source of electrons, and encourages analyte and reagent gas ions to move toward the inlet of the mass spectrometer.[15] Ionization occurs by several possible mechanisms. In the positive mode, the ionization mechanism depends on the reagent gas used. If neon or nitrogen is used, Penning ionization will be dominant. This occurs when the metastable gas atom (M) collides with the analyte (A) and results in the radical molecular cation forming along with a ground-state reagent gas atom and an electron.[16] For this to occur, the analyte must have a lower ionization potential than the energy in the metastable gas atom.

$$M^* + A \rightarrow A^{+\bullet} + M + e^-$$

If helium gas is used, the leading mechanism for positive-ion formation will be the formation of ionized water clusters coupled with proton transfer reactions as shown below:

$$He(2^3S) + H_2O \rightarrow H_2O^{+\bullet} + He(1^1S) + e^-$$

$$H_2O^{+\bullet} + H_2O \rightarrow H_3O^+ + OH\bullet$$

$$H_3O^+ + nH_2O \rightarrow [(H_2O)nH]^+$$

$$[(H_2O)nH]^+ + A \rightarrow AH^+ + nH_2O$$

This results in the formation of the protonated molecular cation of the analyte.

The ionization mechanism in the negative mode is independent of the reagent gas used but sensitivity is dependent on the type of gas used.[15] He gas is the most sensitive, followed by Ne, and then N_2. Negative ionization occurs first by the production of electrons by Penning ionization or surface Penning ionization. These electrons then collide with atmospheric pressure gas and undergo electron capture by atmospheric oxygen. This produces O_2^- which forms anions when it reacts with the sample of interest. The abstracted hydrogen molecular anion or the radical molecular anion can form. Sensitivity is dependent on the reagent gas used because electron formation via Penning ionization is more efficient as gas internal energy increases.

$$M^* + \text{surface} \rightarrow M + \text{surface} + e^-$$

$$e^-_{\text{fast}} + \text{gas} \rightarrow e^-_{\text{slow}}$$

$$e^-_{\text{slow}} + O_2 \rightarrow O_2^-$$

$$O_2^- + A \rightarrow [A\text{-}H]^- \text{ or } A^{-\bullet}$$

Different sample introductions can be used in conjunction with the DART ionization source. In these methods, temperature of the gas emitted by the DART source, heating of the sample, and a combination of both are employed. Differences in methods result in different chemical compounds being desorbed and ionized and therefore detected by the mass spectrometer. Figure S3a displays the linear rail attachment in which the QuickStrip cards are inserted. Samples are dotted on the mesh sample spots and allowed to dry before being placed in the linear rail, which moves the sample spots in front of the DART source at a controlled rate and controlled temperature gas. Figure S3b shows the IonRocket attachment in which the sample is deposited into a copper pot and then placed into the heated stage which heats the sample along a computer programmed temperature gradient.

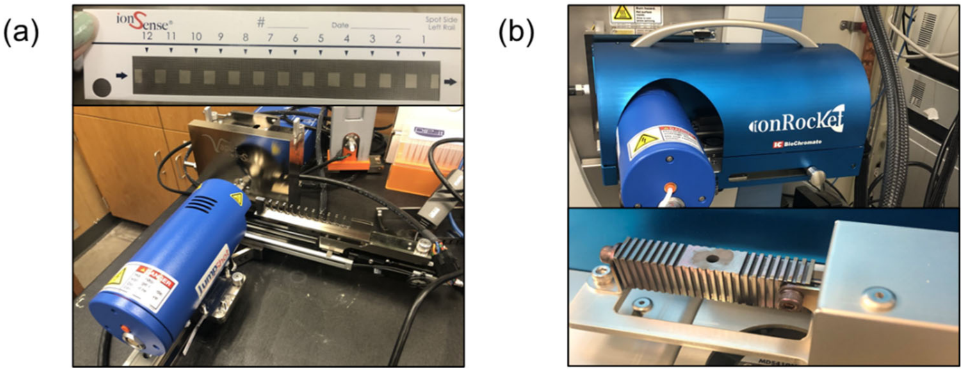

Figure S3. (a) the DART linear rail attachment with QuickStrip sample cards and (b) the IonRocket attachment showing the heating stage and the sample holder.

After data collection, the DART-HRMS datasets were processed as described below.[17] Raw data files were exported from ThermoFisher XCalibur software and deconvoluted using DeconTools AutoProcessor v2.0.7787 (https://github.com/PNNL-Comp-Mass-Spec/DeconTools). This procedure resulted in the lists of experimental values containing m/z values, peak intensity, and full-width-half-maximum (FWHM) for each peak in the mass spectrum. Delta FWHM was then calculated using the following equation:

$$\Delta FWHM = FWHM - 0.00000036({}^{m}/_{z})^{1.61}$$

Outliers were removed by plotting $\Delta FWHM$ versus m/z and manually removing points that did not fall along the curve. Mass to charge values and peak intensity were imported into custom Excel macros that remove C^{13} isotopes and group homologous species based on the first-order (CH_2) and second-order (CH_2, H_2) Kendrick mass defects.[18] Background subtraction for data processing was done separately for each of the DART experiments where different attachment were used. For the linear rail, the sample spectra were subtracted in the ThermoFisher Scientific X-Calibur software. Since there were two sample measurements for each gas temperature, the intensity values were averaged together after the removal of C-13 isotopes. For the IonRocket, a blank and sample mass spectra were generated. They were processed the same up to the point as which isotopes were removed. At that point, the signal-to-noise ratio was calculated by dividing the sample intensity by the blank intensity values. Any values with S/N less than 10 were removed. Molecular formulas were assigned using the MIDAS molecular formula calculator v1.1 (https://nationalmaglab.org/user-facilities/icr/icr-software) with the following elemental limitations, $C_{<50}H_{<100}O_{<25}N_{0\text{-}5}S_{0\text{-}1}$ and a mass tolerance of ± 3 ppm. The assigned formulas were sorted into classes as CHO (CH and CHO), CHON (CHON and CHN), CHOS (CHOS and CHS), and CHONS (CHONS and CHNS).

Supplementary Note 5: Polymerization and oligomerization reaction pathways

Curing of the resin into composite proceeds through peroxide-initiated polymerization. A peroxide initiator begins the reaction by forming free radicals which will propagate more radicals, typically on the ethylene group of the resin monomer. The product is the resin monomer stitched together in long chains to form the corresponding polymer such as polystyrene is formed from the polymerization of styrene as seen in Figure S4a.[19] The analogous polymerization mechanism for the vinyl ester-based resin is shown in Figure S4b.

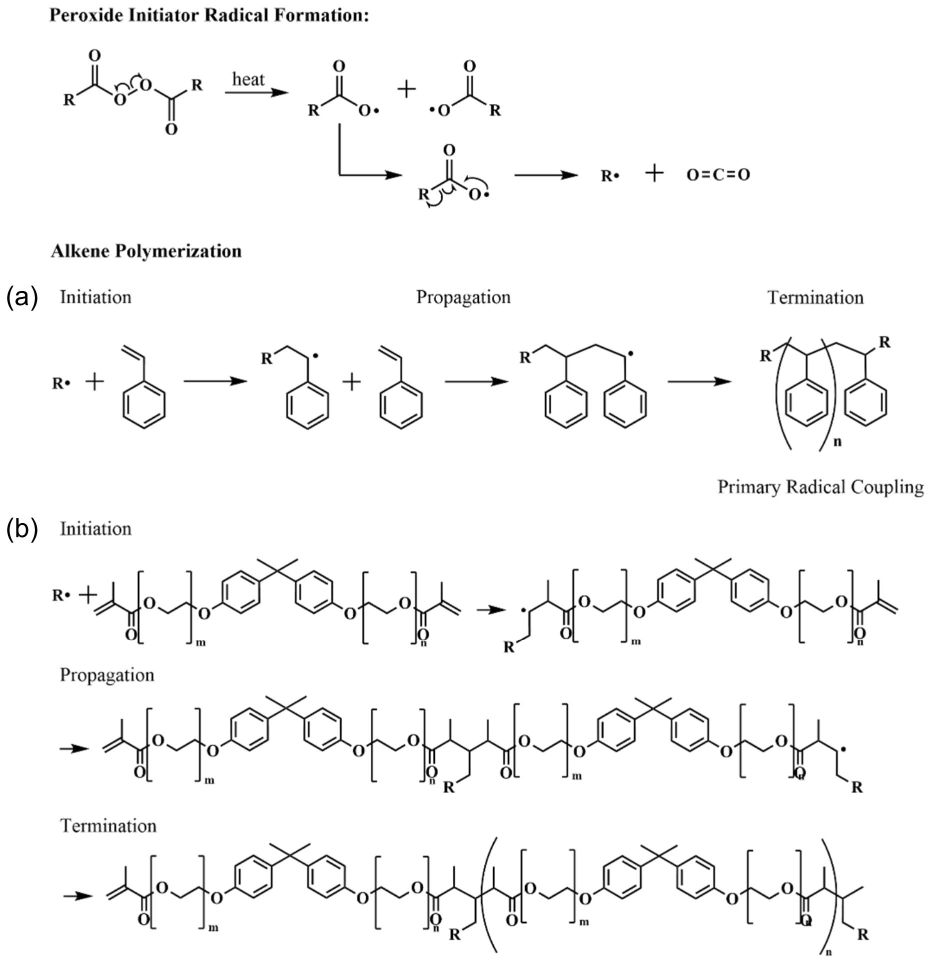

Figure S4. Radical initiated polymerization pathway of (a) styrene and (b) bisphenol A ethoxylate dimethacrylate.

Vinyl ester-based resin are created from an esterification reaction of an epoxy resin and acrylic or methacrylic acids as shown in Figure S5.[20] Common epoxy resin backbones are bisphenol A (BPA), which are used to produce strong and durable plastics.[21]

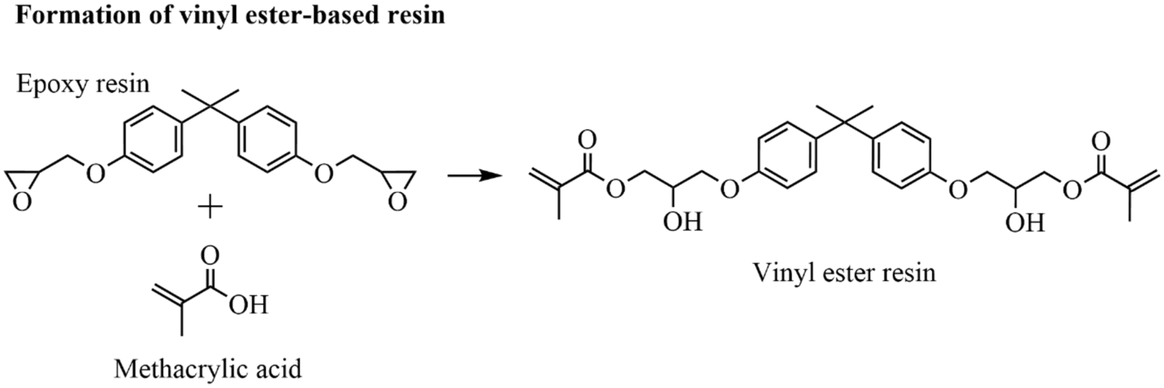

Figure S5. The formation of vinyl ester-based resins from epoxy resin and methacrylic acid.

Because small microplastic particles do not resemble products of intended polymerization, it is likely that they are formed through environmental oligomerization reactions facilitated in drying steam laden waste droplets. These proposed reaction mechanisms are shown in Figure S6 and have been previously reported.[2]

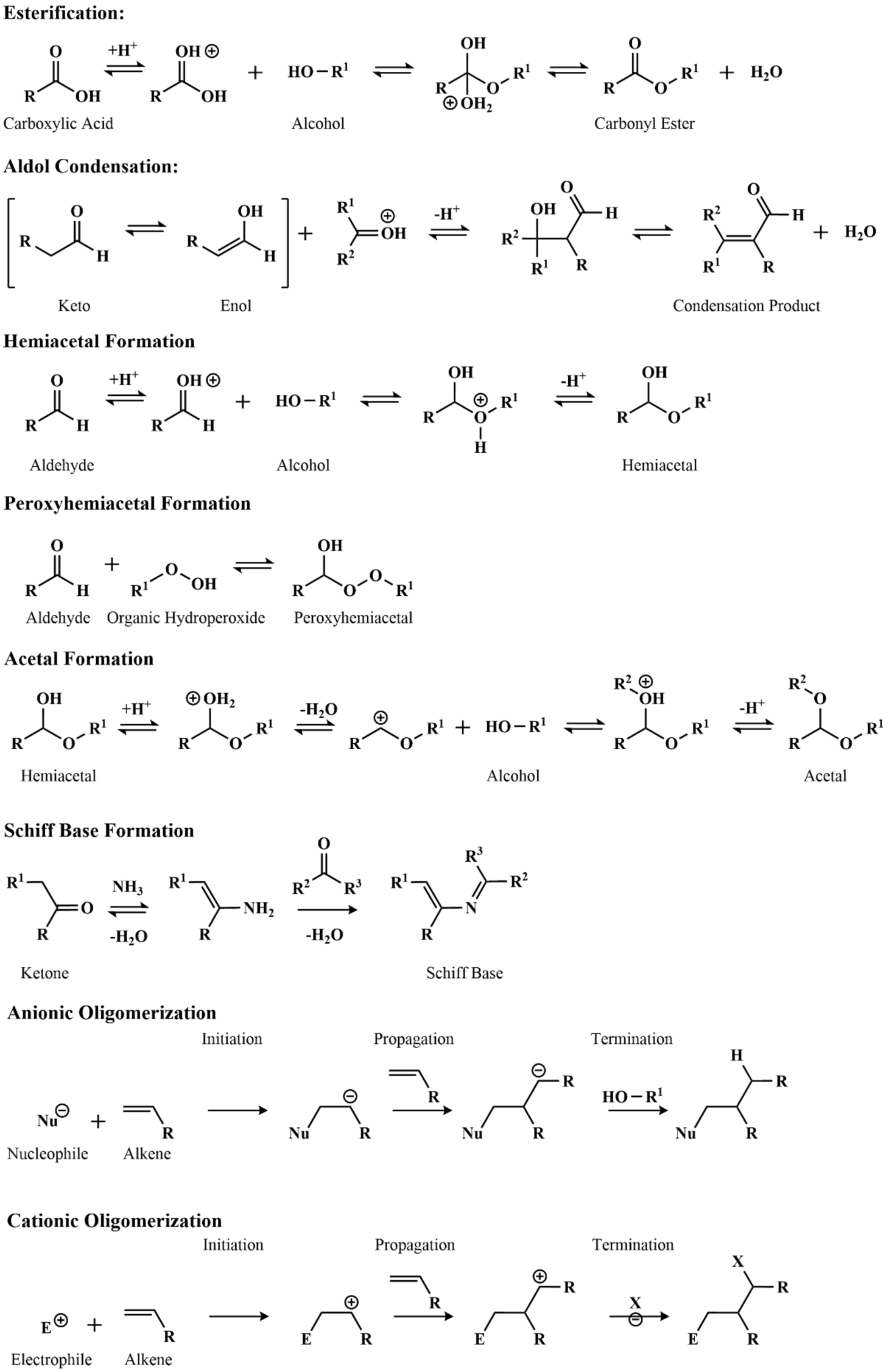

Figure S6. Potential oligomerization pathways occurring in the steam laden waste emissions resulting in the formation of NP particles.[22–27]

Supplementary Note 6: Equations and plots used for DART-HRMS analysis.

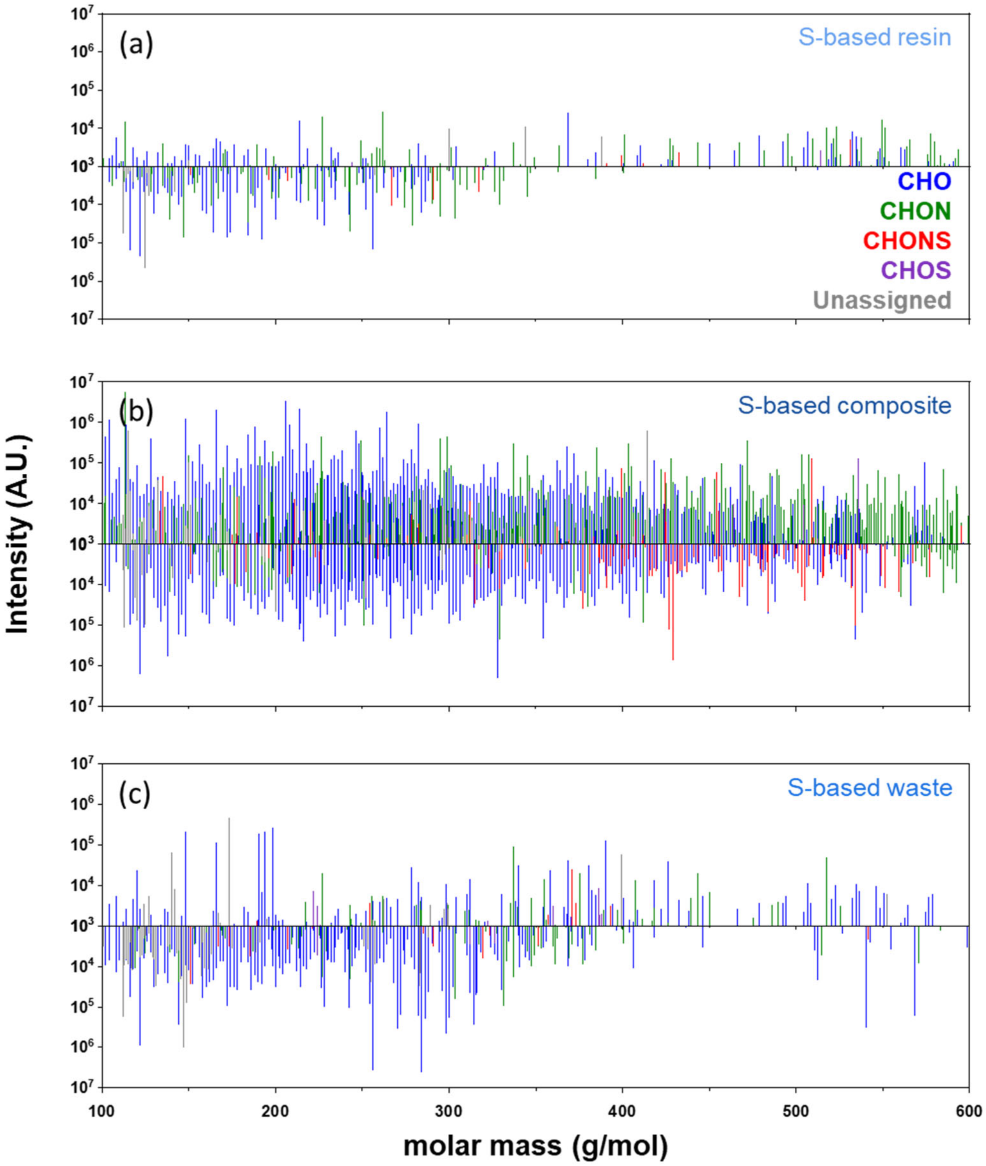

Figure S7. Combined linear rail and IonRocket DART-HRMS spectra for (a) S-based resin, (b) S-based composite, and (c) S-based waste. Peaks are colored by their assigned class.

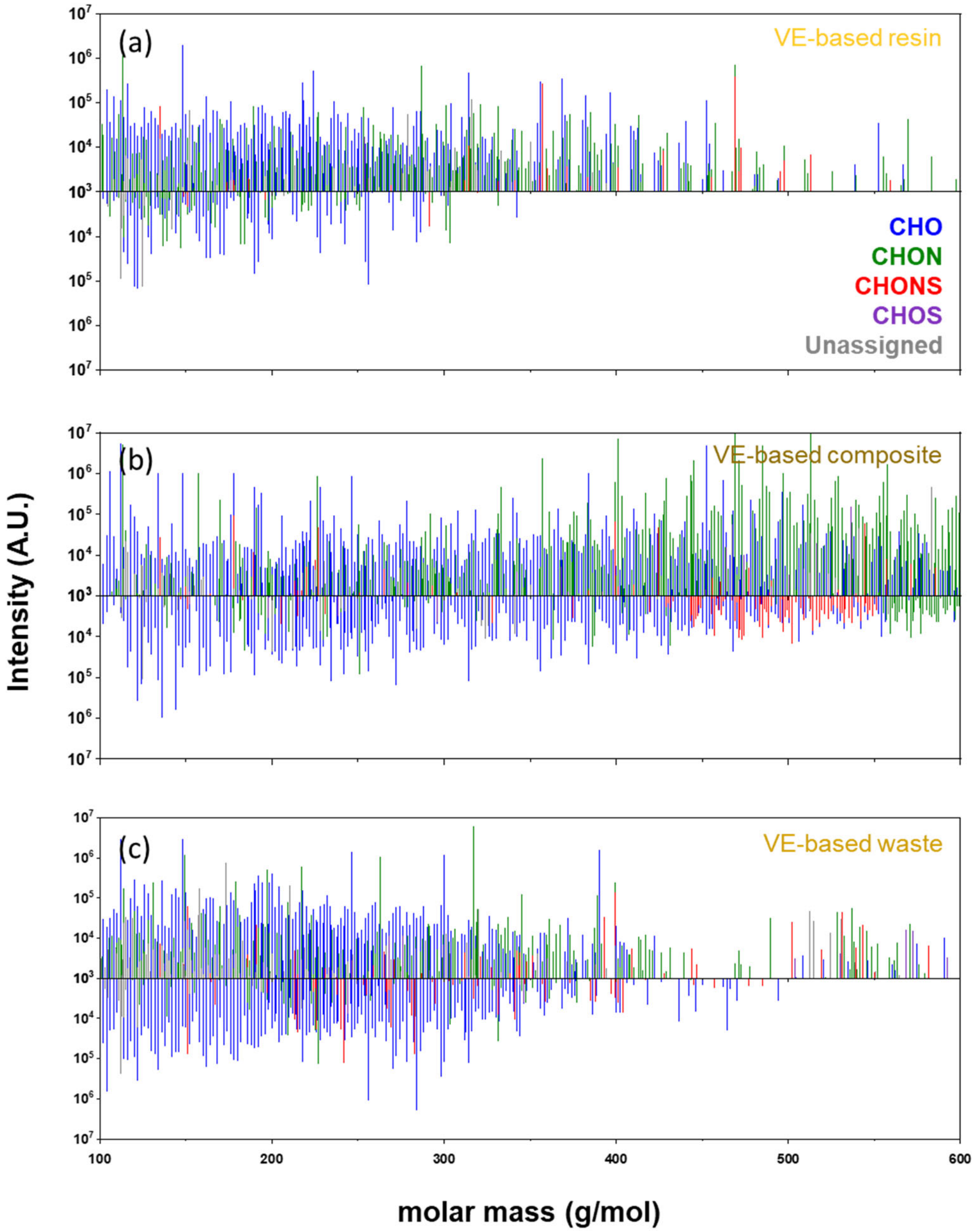

Figure S8. Combined linear rail and IonRocket DART-HRMS spectra for (a) VE-based resin, (b) VE-based composite, and (c) VE-based waste. Peaks are colored by their assigned class.

Double bond equivalency was calculated using the following equation:[28]

$$DBE = C - \frac{H}{2} + \frac{N}{2} + 1$$

The reference lines indicate compounds with structures similar to linear polyenes (DBE = 0.5*C), cata-PAHs (DBE = 0.75*C – 0.5), and fullerene-like hydrocarbons (DBE = 0.9*C).[29] The area below the linear polyene line is considered the “aliphatic” region, while the area between the linear polyene and fullerene-like hydrocarbon line is considered the “aromatic region.”

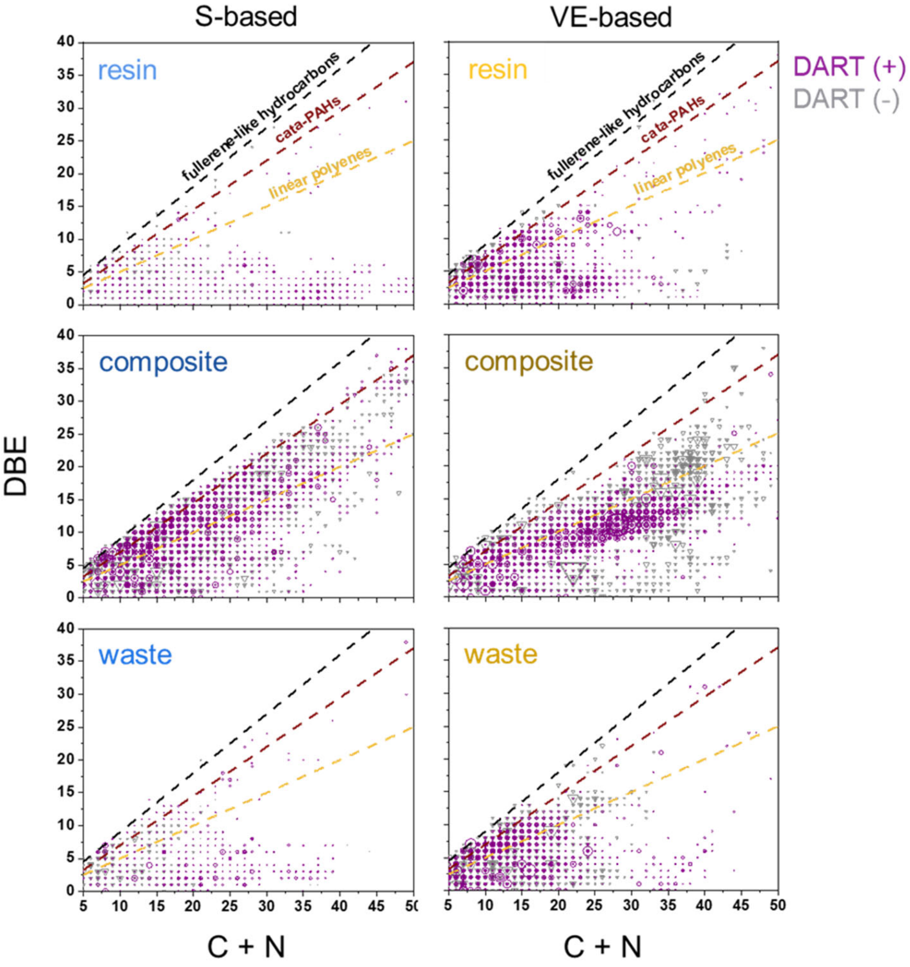

Figure S9. DBE values plotted against the number of carbon and nitrogen atoms assigned for each species. The lines indicate reference values of linear polyenes, DBE = 0.5*C; cata-PAHs, DBE = 0.75*C – 0.5; and fullerene-like hydrocarbons, DBE = 0.9*C. Color of the symbols indicates compounds assigned based on DART(+) and DART(-) detection. Symbols are scaled to the fourth root of the intensity of the corresponding MS peak.

Van Krevelen diagrams are often used to visually analyze chemical species in complex mixtures and are created by plotting H/C versus O/C.[30]

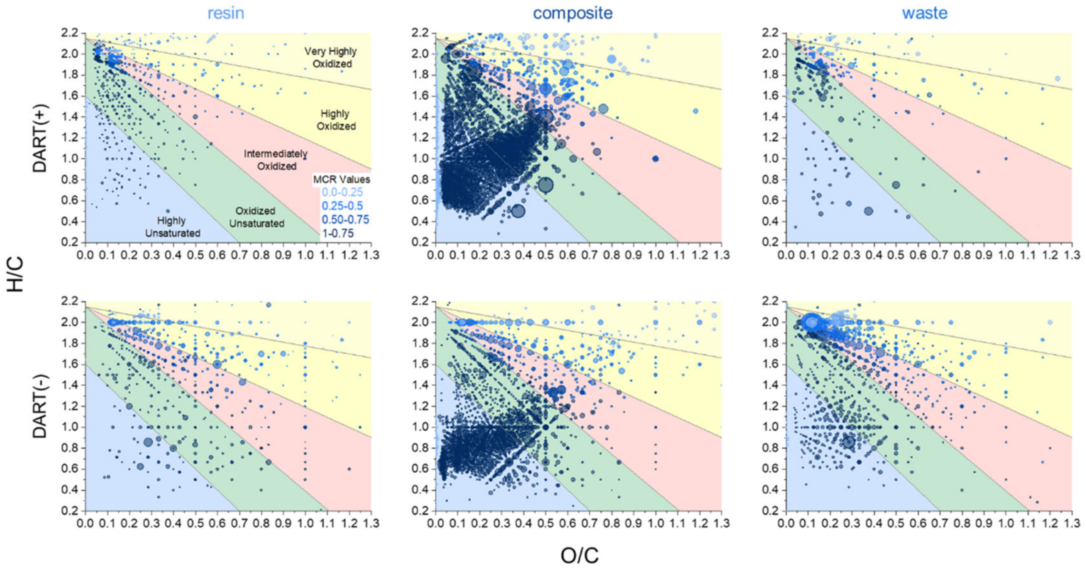

Figure S10. Van Krevelen diagrams of the S-based system for both DART(+) and DART(-) modes. Symbols are color-coded by maximum carbonyl ratio value and scaled to the fourth root of the intensity of the corresponding MS peak.

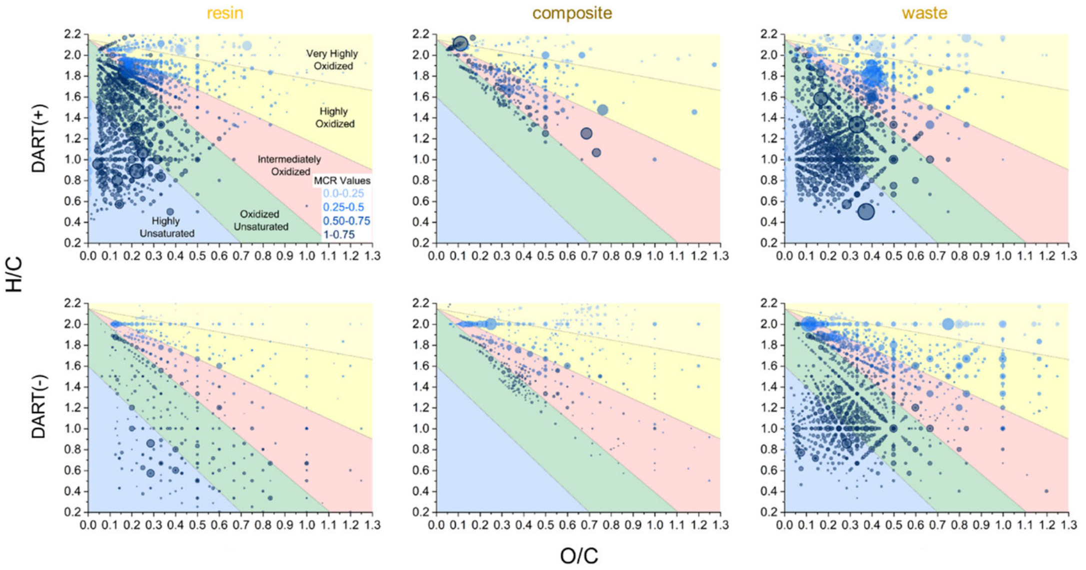

Figure S11. Van Krevelen diagrams of the VE-based system for both DART(+) and DART(-) modes. Symbols are color-coded by maximum carbonyl ratio value and scaled to the fourth root of the intensity of the corresponding MS peak.

The nominal oxidation state of carbon (NOSc) was calculated using an equation from Kroll et al. 2011, extended to include N and S containing compounds.[31,32]

$$OSc = 2\frac{O}{C} + 3\frac{N}{C} + 2\frac{S}{C} - \frac{H}{C}$$

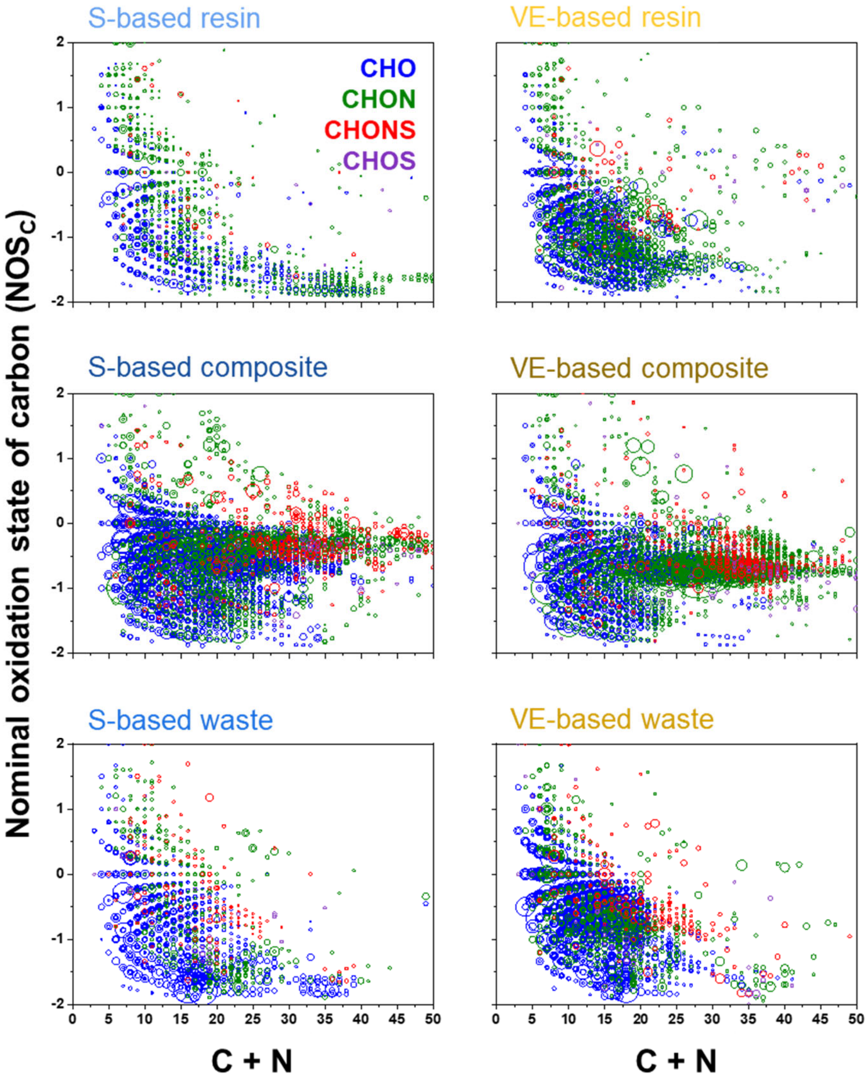

Figure S12. The nominal oxidation of carbon (NOSc) plotted against the number of carbon and nitrogen for each assigned species for the S-based (left) and VE-based system (right). Symbols are scaled by the fourth root of the corresponding mass peak intensities and colored by class.

Volatility indicated by the saturation mass concentration ($\log_{10}C^*_{298K}$) ($\mu g\ m^{-3}$) was calculated using the Molecular Corridors model outlined in Li et al.[33]:

$$log_{10}C *_{298K} = (n_C^0 - n_C)b_C - n_O b_O - 2\frac{n_C n_O}{n_C + n_O} b_{CO} - n_N b_N - n_S b_S$$

In this equation, n_C^0 is the reference carbon number. n_C, n_O, n_N, and n_S are the number of carbon, oxygen, nitrogen, and sulfur atoms, respectively. b_C, b_O, b_N, and b_S are the contribution of each atom to the saturation mass concentration tabulated in Li et al. (2016).[33] b_{CO} is the carbon-oxygen nonideality reported in Donahue et al. (2011).[34]

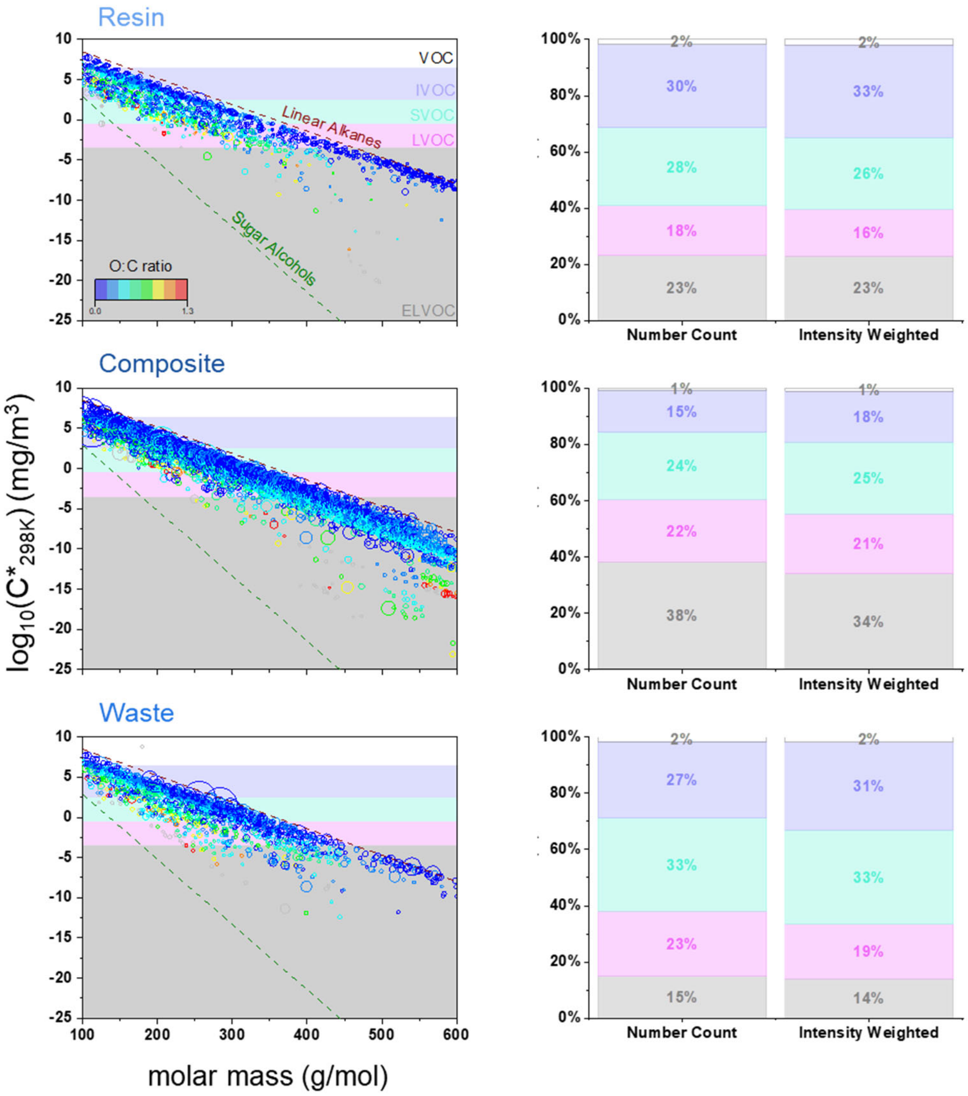

Figure S13. Molecular corridor models and percent contribution of each volatility class for the S-based system. Symbols are scaled by the fourth root of the intensity for the corresponding mass peak signal and colored by O:C ratio.

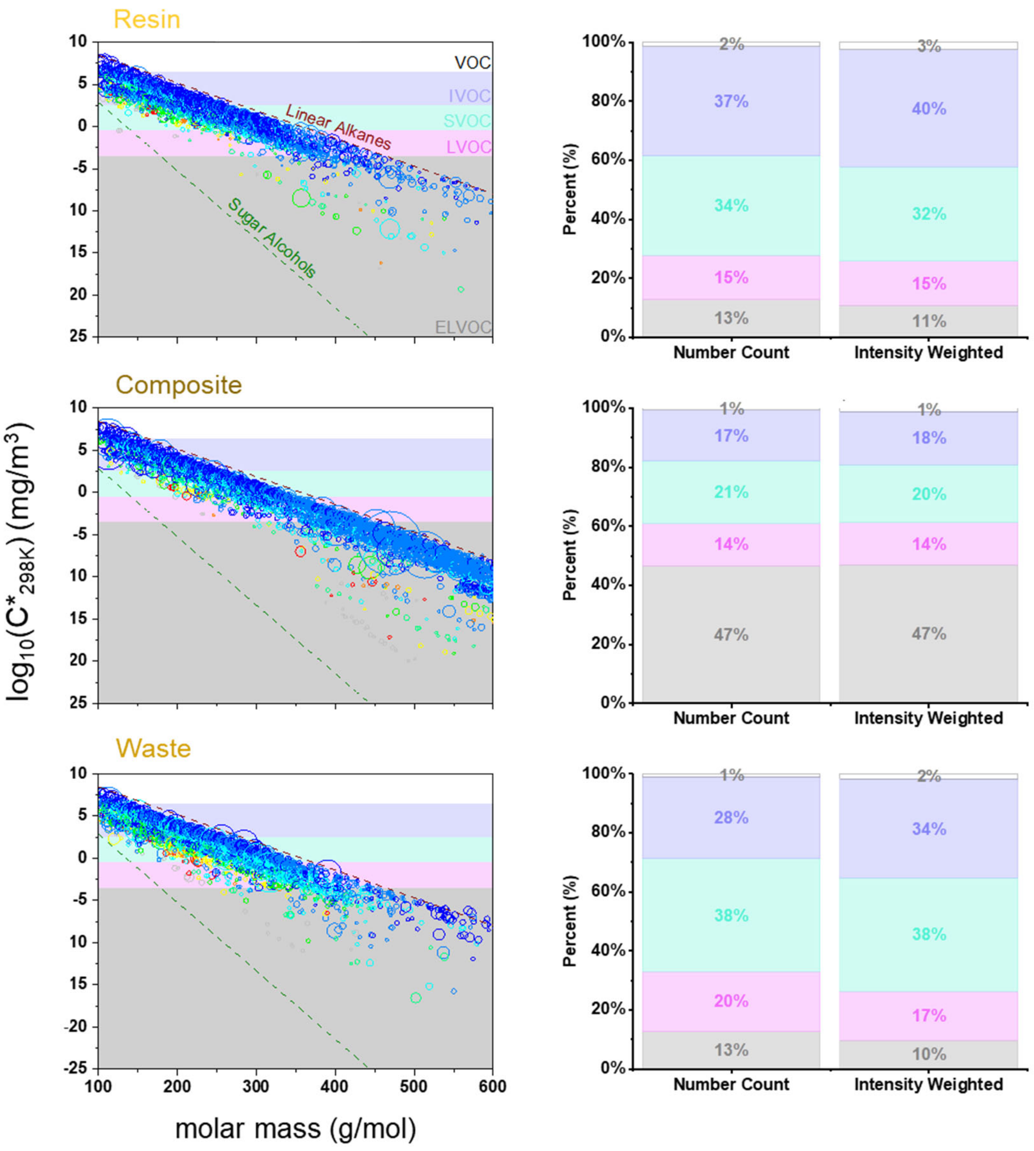

Figure S14. Molecular corridor models and percent contribution of each volatility class for the VE-based system. Symbols are scaled by the fourth root of the intensity for the corresponding mass peak signal and colored by O:C ratio.

The viscosity (η) (Pa s) was calculated using parameters tabulated in DeRieux et al. (2018) and using the equation below:[35]

$$\eta = \eta_{\infty} e^{\frac{T_0 D}{T - T_0}}$$

where η_{∞} is equal to 10^{-5} Pa s, D is the fragility parameter assumed to be 10 based on DeRieux et al. (2018), and T_0 is the Vogel temperature calculated using the equation below.

$$T_0 = \frac{39.17 T_g}{D + 39.17}$$

Where T_g is the glass transition temperature as calculated using the equation below:

$$T_g = (n_C^0 + \ln(n_C)) b_C + \ln(n_H)\, b_H + \ln(n_C) \ln(n_H)\, b_{CH} + \ln(n_O)\, b_O + \ln(n_C) \ln(n_O)\, b_{CO}$$

Supplementary Note 7: Venn diagrams showing the similarities and differences between samples.

a) S-based system

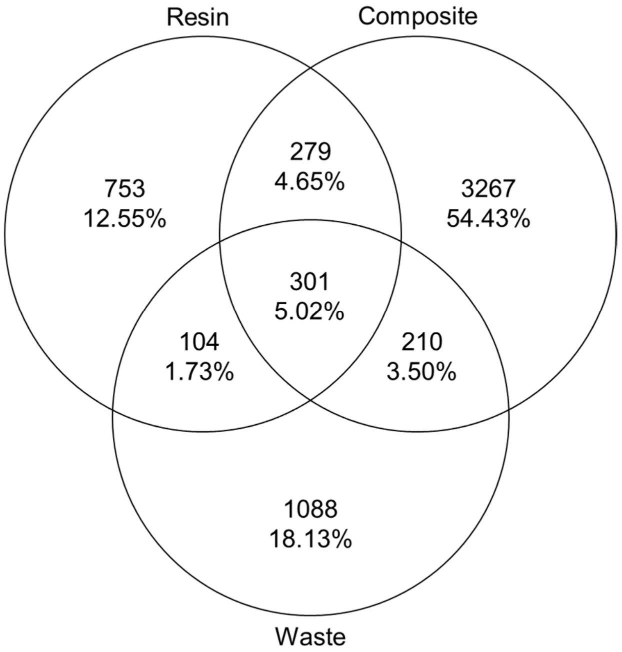

b) VE-based system

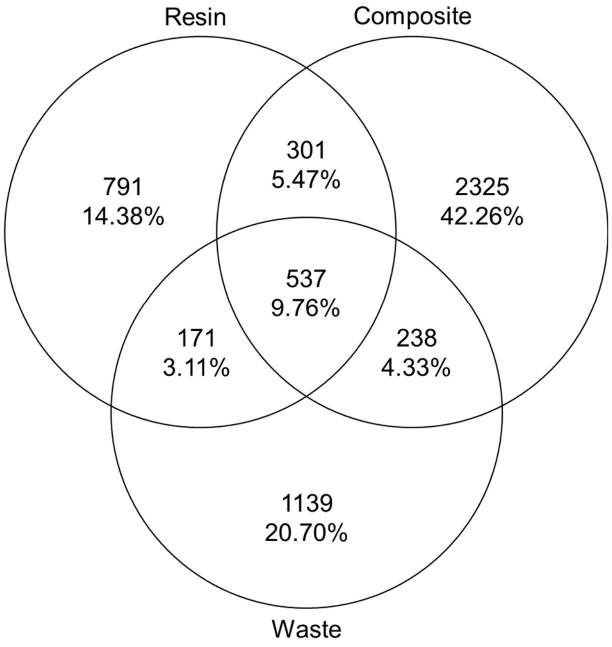

Figure S15. Venn diagram showing the assigned species shared between the resin, composite, and waste for (a) the S-based system and(b) the VE-based system.

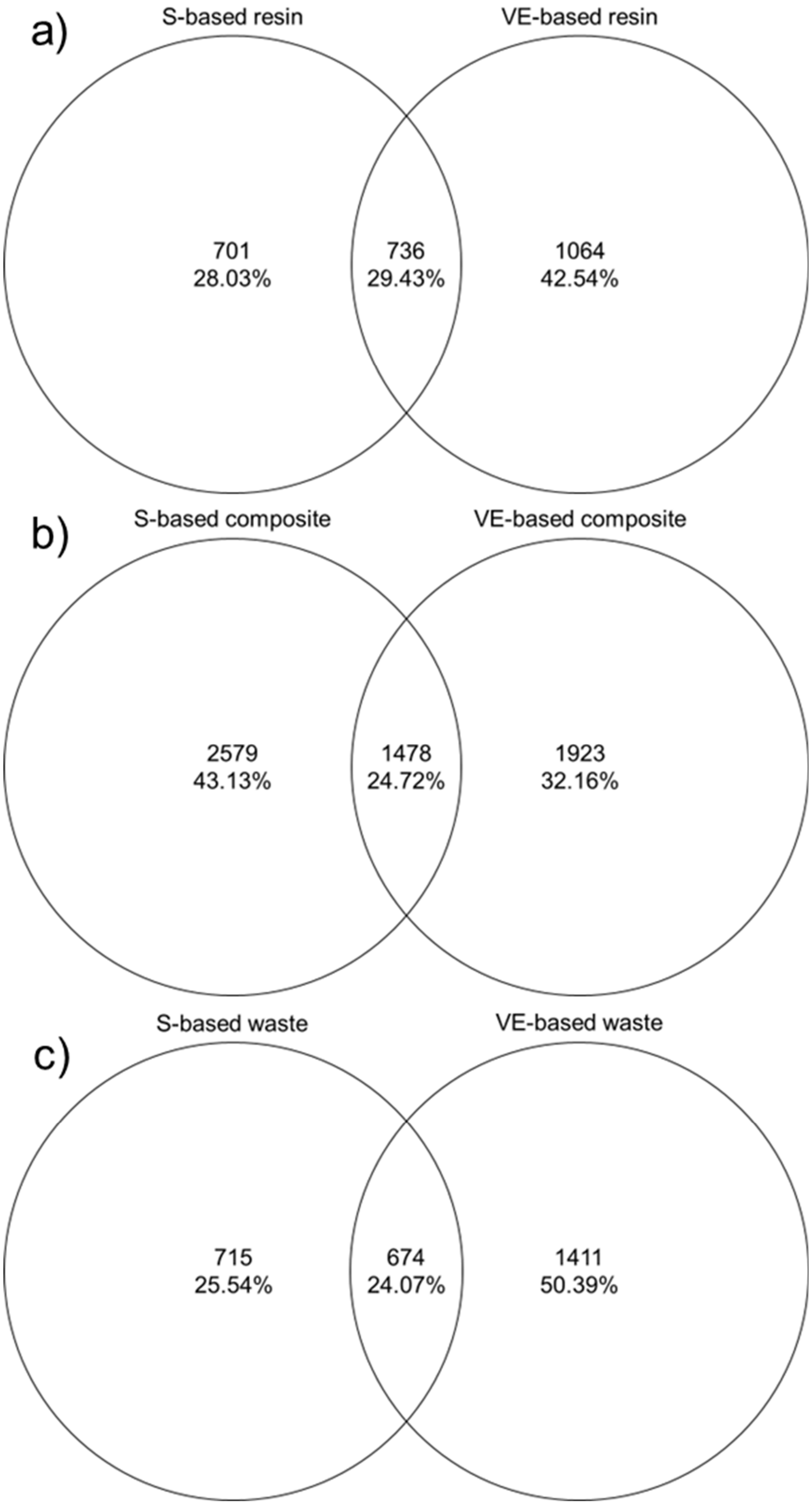

Figure S16. Venn diagrams showing the shared species between the two different systems for the (a) resin, (b) composite, and (c) waste.

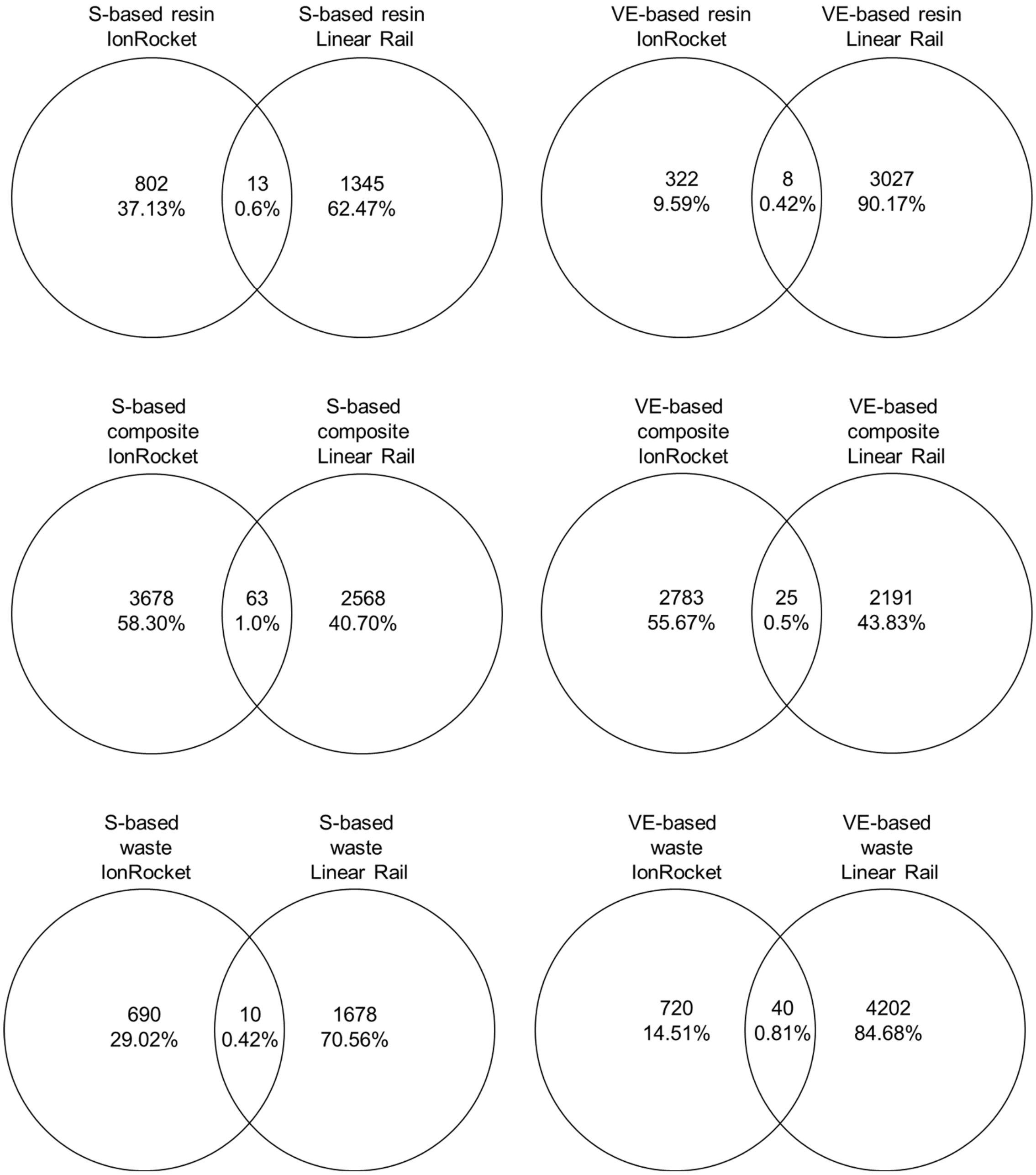

Figure S17. Ven diagrams showing the HRMS features shared between the linear rail and IonRocket DART methods for each of the six samples. m/z values were rounded to four decimal points.

Supplementary Note 8: Table of identified compounds in DART-HRMS.

Table S1. Summary of identified species found in the samples along with their toxicological information.

Neutral Formula	(+) mode m/z	(+) mode error	(-) mode m/z	(-) mode error	Neutral mass	Sample found	Description of possible molecular components
$C_5H_8O_2$	101.0595	1.9			100.0524	VE-based resin	Methyl methacrylate Resin monomer
	101.0597	0.1				VE-based waste	
	101.0597	0.3				S-based resin	
	101.0598	-0.8				S-based composite	
	101.0597	-0.1				S-based waste	
C_8H_8	105.0698	0.5			104.0626	VE-based resin	Styrene Resin monomer
	105.0699	-0.3				VE-based composite	
	105.0699	-0.3				VE-based waste	
	105.0698	0.3				S-based resin	
	105.0700	-0.8				S-based composite	
	105.0698	0.2				S-based waste	
C_7H_6O	107.0491	0.5			106.0419	VE-based resin	Benzaldehyde Oxidized derivative of styrene Decomposition product of peroxide initiators
	107.0491	0.2				VE-based composite	
	107.0491	0.2				VE-based waste	
	107.0490	0.8				S-based resin	
	107.0492	-0.7				S-based composite	
C_8H_{10}	107.0854	1.4			106.0783	VE-based resin	Ethylbenzene[36] Used in the synthesis of styrene Irritant and potential carcinogen
	107.0855	-0.1				VE-based composite	
	107.0856	-0.7				VE-based waste	
	107.0854	0.7				S-based resin	
	107.0856	-0.5				S-based composite	
	107.0855	0.6				S-based waste	

C_7H_8O	109.0648	0.3			108.0575	VE-based resin	Benzyl alcohol[37] Plasticizer and solvent Irritant
	109.0649	-0.8	107.0502	0.0		VE-based composite	
	109.0649	-1.0	107.0501	1.0		VE-based waste	
	109.0648	0.3				S-based resin	
	109.0649	-1.2	107.0502	0.0		S-based composite	
	107.0501	1.0				S-based waste	
$C_6H_6O_2$	111.0440	0.4	109.0294	1.0	110.0368	VE-based resin	Hydroquinone[38] Used in synthesis of substances Suspected teratogen and carcinogen
	111.0441	-0.7	109.0295	0.2		VE-based composite	
	111.0441	-0.1	109.0294	1.3		VE-based waste	
	111.0440	0.6	109.0294	1.2		S-based resin	
	111.0442	-0.9				S-based composite	
			109.0293	1.6		S-based waste	
C_9H_{10}	119.0853	1.7			118.0782	VE-based resin	2-propenyl benzene[39] Little to no known toxicological information
	119.0855	0.1				VE-based composite	
	119.0856	-0.3				VE-based waste	
	119.0855	0.4				S-based resin	
	119.0855	0.4	117.0710	-0.2		S-based composite	
	119.0856	-0.2				S-based waste	
C_8H_8O	121.0647	0.8	119.0501	1.5	120.0575	VE-based resin	Acetophenone Oxidized derivative of styrene Decomposition product of peroxide initiators
	121.0648	0.1	119.0502	0.1		VE-based composite	
	121.0648	0.2	119.0501	1.2		VE-based waste	
	121.0647	0.7	119.0500	1.6		S-based resin	
	121.0648	0.1	119.0503	-0.2		S-based composite	
	121.0648	0.0	119.0501	0.9		S-based waste	
C_9H_{12}	121.1010	1.6			120.0939	VE-based resin	Isopropyl benzene Decomposition product of peroxide initiators
	121.1012	0.1				VE-based composite	
	121.1013	-0.7				VE-based waste	
	121.1011	0.7				S-based resin	
	121.1013	-0.9				S-based composite	
	121.1012	0.1				S-based waste	

$C_7H_6O_2$	123.0439	1.0	121.0294	1.4	122.0368	VE-based resin	Benzoic acid Oxidized derivative of styrene Decomposition product of peroxide initiators
	123.0440	0.3	121.0295	0.3		VE-based composite	
	123.0441	-0.6	121.0293	1.3		VE-based waste	
	123.0439	1.0	121.0293	1.4		S-based resin	
	123.0440	0.4	121.0295	0.3		S-based composite	
	123.0440	0.2	121.0294	1.2		S-based waste	
$C_8H_{10}O$	123.0803	0.9			122.0732	VE-based resin	Phenylethyl alcohol[40] Irritant
	123.0804	0.2				VE-based composite	
	123.0804	0.4	121.0657	1.2		VE-based waste	
	123.0803	0.8				S-based resin	
	123.0804	0.4				S-based composite	
	123.0804	0.4	121.0658	0.6		S-based waste	
$C_8H_{14}O$	127.1116	1.4	125.0970	1.5	126.1045	VE-based resin	4-(1,1-dimethyl) cyclohexanone[41] Little to no known toxicological information
	127.1118	-0.3	125.0971	0.5		VE-based composite	
			125.0970	1.1		VE-based waste	
	127.1116	0.7	125.0970	1.6		S-based resin	
	127.1118	-0.1	125.0971	0.9		S-based composite	
			125.0970	1.3		S-based waste	
$C_8H_{16}O$	129.1274	0.1	127.1127	0.9	128.1201	VE-based resin	4-(1,1-dimethyl) cyclohexanol Irritant
			127.1128	0.1		VE-based composite	
			127.1127	1.0		VE-based waste	
			127.1126	1.5		S-based resin	
			127.1128	0.3		S-based composite	
			127.1127	1.2		S-based waste	
$C_{10}H_{10}$	131.0854	0.7			130.0783	VE-based resin	Di-vinylbenzene[42] Styrene with additional vinyl group Irritant
	131.0856	-0.3				VE-based composite	
	131.0856	-0.4				VE-based waste	
	131.0855	0.4				S-based resin	
	131.0856	-0.2	129.0710	-0.2		S-based composite	

$C_{10}H_{14}$	135.1167	1.0			134.1096	VE-based resin	Tert-butyl benzene[43] Irritant
	135.1168	-0.1				VE-based composite	
	135.1170	-1.4				VE-based waste	
	135.1167	0.7				S-based resin	
	135.1168	0.0				S-based composite	
	135.1168	-0.3				S-based waste	
$C_9H_{16}O$	141.1272	1.0	139.1126	1.3	140.1201	VE-based resin	3,3,5-trimethyl cyclohexanone[44] Irritant Potential mutagen
	141.1273	0.6				VE-based composite	
	141.1271	2.2				VE-based waste	
			139.1127	1.2		S-based resin	
	141.1274	-0.5	139.1128	-0.1		S-based composite	
			139.1128	0.6		S-based waste	
$C_8H_{16}O_2$	145.1222	0.7	143.1075	1.7	144.12	VE-based resin	2-hydroxy-2-methyl-4-heptanone Little to no known toxicological information
			143.1077	0.3		VE-based composite	
			143.1079	-0.9		VE-based waste	
			143.1075	1.6		S-based resin	
$C_8H_4O_3$	149.0232	0.7			148.0161	VE-based resin	Phthalic anhydride[45] Resin monomer Plasticizers Irritant
	149.0233	-0.1	147.0089	-0.9		VE-based composite	
	149.0234	-0.3	148.0165	-0.5		VE-based waste	
	149.0233	0.4				S-based resin	
	149.0235	-1.1	148.0167	-0.5		S-based composite	
	149.0234	-0.5	148.0165	0.4		S-based waste	
$C_9H_{10}O_2$	151.0753	0.6	149.0606	1.5	150.0681	VE-based resin	1-phenyl-1-hydroxy-2-propanone Little to no known toxicological information
	151.0753	0.1	149.0607	0.4		VE-based composite	
	151.0753	0.2	149.0606	1.1		VE-based waste	
	151.0752	0.7	149.0606	1.4		S-based resin	
	151.0754	-0.3	149.0608	0.1		S-based composite	
	151.0753	0.3	149.0606	1.0		S-based waste	

C_7H_5NOS	152.0164 152.0163	0.1 0.8	150.0017 150.0018 150.0017 150.0017 150.0019 150.0017	1.4 0.4 1.2 1.6 0.1 1.2	151.0092	VE-based resin VE-based composite VE-based waste S-based resin S-based composite S-based waste	2(3H)-benzothiazolone Little to no known toxicological information
$C_{10}H_{18}O$	155.1428 155.1429	1.8 0.8	153.1284 153.1285	0.8 0.0	154.1358	VE-based resin VE-based waste S-based composite S-based waste	4-tert-butylcyclohexanone Decomposition product of peroxide initiators
$C_8H_4O_4$	165.0183 165.0184	-0.1 -0.8	163.0035 163.0038 163.0036 163.0035 163.0037 163.0036	1.2 -0.8 0.4 1.1 -0.3 0.6	164.0110	VE-based resin VE-based composite VE-based waste S-based resin S-based composite S-based waste	Styrene polyester Resin component
$C_{14}H_{10}$	179.0854 179.0854 179.0855 178.0776	0.7 0.6 0.1 0.3			178.0783	VE-based resin VE-based composite VE-based waste S-based composite	Phenanthrene[46] Polycyclic aromatic hydrocarbon Recognized as an aquatic hazard
$C_{12}H_{10}O_2$	187.0753 187.0752 187.0754 187.0753	0.5 0.6 -0.1 0.2	185.0606 185.0610 185.0608 185.0609 185.0608	0.9 -1.0 0.1 -0.8 0.2	186.0681	VE-based resin VE-based composite VE-based waste S-based composite S-based waste	Oxidized polycyclic aromatic hydrocarbon
$C_{11}H_{12}O_3$	193.0858 193.0858 193.0860 193.0859	0.4 0.4 -0.2 -0.1	191.0712 191.0715 191.0713 191.0715 191.0714	0.8 -0.9 0.3 -0.7 0.1	192.0787	VE-based resin VE-based composite VE-based waste S-based composite S-based waste	Ethyl benzoylacetate[47] Little to no known toxicological information

$C_{12}H_{16}O_2$	193.1222	0.6			192.1150	VE-based resin	4,7-methano-1H-indenol, hexahydro acetate Little to no known toxicological information
	193.1223	-0.2	191.1078	-0.2		VE-based composite	
	193.1224	-0.4	191.1077	0.4		VE-based waste	
	193.1222	0.6				S-based resin	
	193.1224	-0.8	191.1079	-0.7		S-based composite	
			191.1077	0.4		S-based waste	
$C_{10}H_{14}O_4$	199.0963	1.1	197.0818	0.8	198.0892	VE-based resin	Ethylene glycol dimethacrylate[48] Resin monomer Irritant and potential mutagen
	199.0964	0.2	197.0820	-0.5		VE-based composite	
	199.0965	-0.2	197.0819	-0.1		VE-based waste	
	199.0964	0.7	197.0817	1.1		S-based resin	
	199.0966	-0.5	197.0820	-0.3		S-based composite	
			197.0817	1.2		S-based waste	
$C_{12}H_{10}O_3$	203.0701	0.9			202.0630	VE-based resin	Styrene-maleic anhydride Resin monomer
			201.0559	-1.1		VE-based composite	
	203.0702	0.1	201.0558	-0.1		VE-based waste	
	203.0702	0.2	201.0559	-0.9		S-based composite	
			201.0558	-0.3		S-based waste	
$C_{16}H_{10}$	202.0776	0.2			202.0783	S-based composite	Pyrene Polycyclic aromatic hydrocarbon
$C_{11}H_{10}O_4$	207.0650	0.8			206.0579	VE-based resin	Methyl vinyl ester terephthalic acid Monomer
	207.0652	0.2	205.0508	-0.8		VE-based composite	
	207.0652	-0.2	205.0506	0.1		VE-based waste	
	207.0651	0.5	205.0504	0.9		S-based resin	
	207.0652	0.2	205.0507	-0.2		S-based composite	
			205.0506	0.1		S-based waste	
$C_{13}H_{22}O_2$	211.1690	1.2			210.1611	VE-based resin	4-tertbutyl cyclohexylacrylate[49] Little to no known toxicological information
	211.1692	0.3	209.1547	-0.2		VE-based composite	
	211.1691	0.7	209.1545	0.9		S-based resin	
	211.1694	-0.8	209.1548	-0.5		S-based composite	

$C_{10}H_{15}NO_2S$	214.0895	-0.5	212.0751	-0.2	213.0824	VE-based waste	N-butyl-benzene sulfonamide Plasticizer Little to no known toxicological information[50]
			212.0751	-0.3		S-based waste	
$C_{12}H_{24}O_3$			215.1650	1.3	216.1726	VE-based resin	Tert-butyl peroxy-2-ethylhexanoate[51] Radical initiator
			215.1653	-0.1		VE-based composite	
			215.1653	0.0		VE-based waste	
			215.1650	1.2		S-based resin	
			215.1653	-0.3		S-based composite	
			215.1653	-0.2		S-based waste	
$C_{15}H_{24}O$	221.1897	1.1			220.1827	VE-based resin	Butylated hydroxytoluene Little to no known toxicological information
	221.1898	0.9				VE-based composite	
			219.1754	0.0		VE-based waste	
	221.1899	0.4				S-based resin	
	220.1822	-0.4	219.1754	0.0		S-based waste	
$C_{12}H_{14}O_4$	223.0965	-0.2	221.0817	1.1	222.0892	VE-based resin	Diethyl phthalate[52] Plasticizer Little to no known toxicological information
	223.0963	0.8	221.0820	-0.6		VE-based composite	
	223.0964	0.1	221.0820	-0.2		VE-based waste	
			221.0818	0.4		S-based resin	
	223.0963	0.7	221.0820	-0.3		S-based composite	
			221.0820	-0.3		S-based waste	
$C_{16}H_{14}O$	223.1116	0.4			222.1045	VE-based resin	Oxidized polycyclic aromatic hydrocarbon
	223.1114	1.5				VE-based composite	
	223.1118	-0.1				VE-based waste	
	223.1117	0.2	221.0973	-0.5		S-based composite	

$C_{12}H_{20}O_4$	229.1433	0.6	227.1288	0.4	228.1362	VE-based resin	Dibutyl maleate Monomer Little to no known toxicological information
	229.1434	0.2	227.1290	-0.5		VE-based composite	
	229.1435	-0.2	227.1290	-0.7		VE-based waste	
			227.1288	0.3		S-based resin	
	229.1433	0.4	227.1291	-1.2		S-based composite	
			227.1291	-0.8		S-based waste	
$C_{20}H_{12}$	253.1010	0.5			252.0939	S-based composite	Benzopyrene Polycyclic aromatic hydrocarbon Suspected carcinogen
$C_{12}H_{14}O_6$	255.0862	0.6			254.0790	VE-based composite	Bis(2-hydroxyethyl) ester Intermediate in the production of PET
	255.0864	-0.2	253.0720	-0.8		VE-based waste	
	255.0862	0.4	253.0719	-0.6		S-based composite	
$C_{16}H_{32}O_2$	257.2472	1.3	255.2328	0.6	256.2402	VE-based resin	n-hexadecanoic acid Classified as a nonhazardous substance
	257.2472	1.0	255.2328	0.6		VE-based composite	
	257.2472	1.0	255.2331	-0.5		VE-based waste	
	257.2474	0.6	255.2327	0.8		S-based resin	
	257.2473	0.9	255.2328	0.4		S-based composite	
	257.2476	-0.2	255.2331	-0.7		S-based waste	
$C_{16}H_{22}O_4$	279.1587	1.4			278.1518	VE-based resin	Dibutyl phthalate[53] Plasticizers Endocrine disrupting compound, potential carcinogen and teratogen
	279.1585	2.1	277.1446	-0.3		VE-based composite	
	279.1591	-0.1	277.1446	-0.2		VE-based waste	
	279.1590	0.5				S-based resin	
	279.1587	1.4	277.1446	-0.3		S-based composite	
	279.1591	-0.2	277.1448	-1.0		S-based waste	

$C_{18}H_{36}O_2$	285.2785	1.2	283.2640	0.7	284.2715	VE-based resin	Octadecanoic acid Softens plastics Classified as nonhazardous
			283.2642	0.2		VE-based composite	
	285.2788	-0.1	283.2643	-0.2		VE-based waste	
			283.2639	1.1		S-based resin	
			283.2642	0.3		S-based composite	
	285.2789	-0.3	283.2643	-0.4		S-based waste	
$C_{15}H_{24}O_6$	301.1644	0.7			300.1573	VE-based resin	Triproylene glycol diacrylate Resin monomer
	301.1643	0.9				VE-based composite	
	301.1645	0.3	299.1500	0.1		VE-based waste	
	301.1644	0.6	299.1498	0.7		S-based resin	
			299.1500	-0.1		S-based waste	
$C_{17}H_{34}O_4$			301.2382	0.9	302.2457	VE-based resin	1,1-di(tert-butyl-peroxy)-3,3,5-trimethyl cyclohexane Peroxide initiator
			301.2385	-0.3		VE-based composite	
			301.2385	-0.2		VE-based waste	
			301.2381	1.0		S-based resin	
			301.2384	0.0		S-based composite	
			301.2385	-0.2		S-based waste	
$C_{19}H_{20}O_4$	313.1428	1.9			312.1362	VE-based resin	Butyl benzyl phthalate[54] Plasticizer Endocrine disrupting compound, potential carcinogen and teratogen
			311.1292	-1.1		VE-based composite	
	313.1435	-0.2	311.1290	-0.2		VE-based waste	
	313.1432	0.7				S-based resin	
	313.1428	1.9	311.1291	-0.7		S-based composite	
			311.1290	-0.4		S-based waste	
$C_{21}H_{24}O_4$	341.1744	0.9	339.1597	1.3	340.1675	VE-based resin	Bisphenol A diglycidyl ether[55] Component of epoxy resin Irritant, potential mutagen, endocrine disrupting compound
	341.1745	0.6				VE-based composite	
	341.1745	0.7				VE-based waste	
	341.1745	0.7	339.1604	-0.7		S-based composite	

$C_{24}H_{38}O_4$	391.2839 391.2838 391.2839 391.2839 391.2842	0.8 1.2 1.1 0.9 0.3			390.2770	VE-based resin VE-based waste S-based resin S-based composite S-based waste	Di(2-ethylhexyl) phthalate[56] or Diisooctyl phthalate[57] Plasticizer Endocrine disrupting compound, potential carcinogen and teratogen
$C_{22}H_{38}O_6$	399.2737	0.9			398.2668	S-based resin	Bis(4-tert-butylcyclohexyl) peroxydicarbonate Perkadox16 Radical initiator
$C_{30}H_{50}$	411.3983 411.3986	0.5 -0.2			410.3913	S-based resin S-based waste	Squalene Little to no known toxicological information

References

1 S. M. Teimouri Sendesi, K. Ra, E. N. Conkling, B. E. Boor, Md. Nuruddin, J. A. Howarter, J. P. Youngblood, L. M. Kobos, J. H. Shannahan, C. T. Jafvert and A. J. Whelton, Worksite Chemical Air Emissions and Worker Exposure during Sanitary Sewer and Stormwater Pipe Rehabilitation Using Cured-in-Place-Pipe (CIPP), *Environ. Sci. Technol. Lett.*, 2017, **4**, 325–333.

2 A. C. Morales, J. M. Tomlin, C. P. West, F. A. Rivera-Adorno, B. N. Peterson, S. A. L. Sharpe, Y. Noh, S. M. T. Sendesi, B. E. Boor, J. A. Howarter, R. C. Moffet, S. China, B. T. O'Callahan, P. Z. El-Khoury, A. J. Whelton and A. Laskin, Atmospheric emission of nanoplastics from sewer pipe repairs, *Nat. Nanotechnol.*, 2022, **17**, 1171–1177.

3 S. M. Teimouri Sendesi, Y. Noh, M. Nuruddin, B. E. Boor, J. A. Howarter, J. P. Youngblood, C. T. Jafvert and A. J. Whelton, An emerging mobile air pollution source: outdoor plastic liner manufacturing sites discharge VOCs into urban and rural areas, *Environ. Sci.: Processes Impacts*, 2020, **22**, 1828–1841.

4 R. C. Moffet, A. V. Tivanski and M. K. Gilles, *Scanning transmission X-ray microscopy: Applications in atmospheric aerosol research*, Lawrence Berkeley National Lab.(LBNL), Berkeley, CA (United States), 2011.

5 T. Hemraj-Benny, S. Banerjee, S. Sambasivan, M. Balasubramanian, D. A. Fischer, G. Eres, A. A. Puretzky, D. B. Geohegan, D. H. Lowndes, W. Han, J. A. Misewich and S. S. Wong, Near-Edge X-ray Absorption Fine Structure Spectroscopy as a Tool for Investigating Nanomaterials, *Small*, 2006, **2**, 26–35.

6 R. C. Moffet, T. Henn, A. Laskin and M. K. Gilles, Automated Chemical Analysis of Internally Mixed Aerosol Particles Using X-ray Spectromicroscopy at the Carbon K-Edge †, *Anal. Chem.*, 2010, **82**, 7906–7914.

7 R. C. Moffet, T. C. Rödel, S. T. Kelly, X. Y. Yu, G. T. Carroll, J. Fast, R. A. Zaveri, A. Laskin and M. K. Gilles, Spectro-microscopic measurements of carbonaceous aerosol aging in Central California, *Atmos. Chem. Phys.*, 2013, **13**, 10445–10459.

8 R. C. Moffet, R. E. O'Brien, P. A. Alpert, S. T. Kelly, D. Q. Pham, M. K. Gilles, D. A. Knopf and A. Laskin, Morphology and mixing of black carbon particles collected in central California during the CARES field study, *Atmos. Chem. Phys.*, 2016, **16**, 14515–14525.

9 M. Fraund, D. J. Bonanno, S. China, D. Q. Pham, D. Veghte, J. Weis, G. Kulkarni, K. Teske, M. K. Gilles, A. Laskin and R. C. Moffet, *Optical properties and composition of viscous organic particles found in the Southern Great Plains*, Aerosols/Field Measurements/Troposphere/Chemistry (chemical composition and reactions), 2020.

10 J. M. Tomlin, K. A. Jankowski, F. A. Rivera-Adorno, M. Fraund, S. China, B. H. Stirm, R. Kaeser, G. S. Eakins, R. C. Moffet, P. B. Shepson and A. Laskin, Chemical Imaging of Fine Mode Atmospheric Particles Collected from a Research Aircraft over Agricultural Fields, *ACS Earth Space Chem.*, 2020, **4**, 2171–2184.

11 R. J. Hopkins, A. V. Tivanski, B. D. Marten and M. K. Gilles, Chemical bonding and structure of black carbon reference materials and individual carbonaceous atmospheric aerosols, *Journal of Aerosol Science*, 2007, **38**, 573–591.

12 A. Zelenyuk, D. Imre, J. Wilson, Z. Zhang, J. Wang and K. Mueller, Airborne Single Particle Mass Spectrometers (SPLAT II & miniSPLAT) and New Software for Data Visualization and Analysis in a Geo-Spatial Context, *J. Am. Soc. Mass Spectrom.*, 2015, **26**, 257–270.

13 A. Zelenyuk, J. Yang, D. Imre and E. Choi, Achieving Size Independent Hit-Rate in Single Particle Mass Spectrometry, *Aerosol Science and Technology*, 2009, **43**, 305–310.

14 J. H. Gross, Direct analysis in real time—a critical review on DART-MS, *Anal Bioanal Chem*, 2014, **406**, 63–80.

15 R. B. Cody, J. A. Laramee, J. M. Nilles and H. D. Durst, Direct analysis in real time (DART) mass spectrometry, *JEOL news*, 2005, **40**, 8–12.

16 F. M. Penning, �ber Ionisation durch metastabile Atome, *Naturwissenschaften*, 1927, **15**, 818–818.

17 C. P. West, H. Yun-Jung, K. T. MacFeely, S. M. Huston, B. P. Aridjis-Olivos, A. C. Morales and A. Laskin, Volatility Measurements of Individual Components in Organic Aerosol Mixtures Using Temperature-Programmed Desorption-Direct Analysis in Real Time-High Resolution Mass Spectrometry, *Analytical Chemistry*.

18 P. J. Roach, J. Laskin and A. Laskin, Higher-Order Mass Defect Analysis for Mass Spectra of Complex Organic Mixtures, *Anal. Chem.*, 2011, **83**, 4924–4929.

19 D. B. Priddy, in *Polymer Synthesis*, Springer-Verlag, Berlin/Heidelberg, 1994, vol. 111, pp. 67–114.

20 H. Q. Pham and M. J. Marks, in *Ullmann's Encyclopedia of Industrial Chemistry*, ed. Wiley-VCH Verlag GmbH & Co. KGaA, Wiley-VCH Verlag GmbH & Co. KGaA, Weinheim, Germany, 2005, p. a09_547.pub2.

21 S. A. Vogel, The Politics of Plastics: The Making and Unmaking of Bisphenol A "Safety", *Am J Public Health*, 2009, **99**, S559–S566.

22 H. Kimura, A simple method for the anionic polymerization of ?-carbonyl acids in water, *J. Polym. Sci. A Polym. Chem.*, 1998, **36**, 189–193.

23 P. J. Ziemann, Formation of Alkoxyhydroperoxy Aldehydes and Cyclic Peroxyhemiacetals from Reactions of Cyclic Alkenes with O_3 in the Presence of Alcohols, *J. Phys. Chem. A*, 2003, **107**, 2048–2060.

24 T. B. Nguyen, P. J. Roach, J. Laskin, A. Laskin and S. A. Nizkorodov, Effect of humidity on the composition of isoprene photooxidation secondary organic aerosol, *Atmos. Chem. Phys.*, 2011, **11**, 6931–6944.

25 R. Zhao, A. K. Y. Lee, R. Soong, A. J. Simpson and J. P. D. Abbatt, Formation of aqueous-phase α-hydroxyhydroperoxides (α-HHP): potential atmospheric impacts, *Atmos. Chem. Phys.*, 2013, **13**, 5857–5872.

26 J. Laskin, A. Laskin, S. A. Nizkorodov, P. Roach, P. Eckert, M. K. Gilles, B. Wang, H. J. (Julie) Lee and Q. Hu, Molecular Selectivity of Brown Carbon Chromophores, *Environ. Sci. Technol.*, 2014, **48**, 12047–12055.

27 H. Herrmann, T. Schaefer, A. Tilgner, S. A. Styler, C. Weller, M. Teich and T. Otto, Tropospheric Aqueous-Phase Chemistry: Kinetics, Mechanisms, and Its Coupling to a Changing Gas Phase, *Chem. Rev.*, 2015, **115**, 4259–4334.

28 F. W. McLafferty and F. Turecek, *Interpretation of mass spectra*, University science books, 1993.

29 V. V. Lobodin, A. G. Marshall and C. S. Hsu, Compositional Space Boundaries for Organic Compounds, *Anal. Chem.*, 2012, **84**, 3410–3416.

30 S. Kim, R. W. Kramer and P. G. Hatcher, Graphical Method for Analysis of Ultrahigh-Resolution Broadband Mass Spectra of Natural Organic Matter, the Van Krevelen Diagram, *Anal. Chem.*, 2003, **75**, 5336–5344.

31 J. H. Kroll, N. M. Donahue, J. L. Jimenez, S. H. Kessler, M. R. Canagaratna, K. R. Wilson, K. E. Altieri, L. R. Mazzoleni, A. S. Wozniak, H. Bluhm, E. R. Mysak, J. D. Smith, C. E. Kolb and D. R. Worsnop, Carbon oxidation state as a metric for describing the chemistry of atmospheric organic aerosol, *Nature Chem*, 2011, **3**, 133–139.

32 J. H. Kroll, C. Y. Lim, S. H. Kessler and K. R. Wilson, Heterogeneous Oxidation of Atmospheric Organic Aerosol: Kinetics of Changes to the Amount and Oxidation State of Particle-Phase Organic Carbon, *J. Phys. Chem. A*, 2015, **119**, 10767–10783.

33 Y. Li, U. Pöschl and M. Shiraiwa, Molecular corridors and parameterizations of volatility in the chemical evolution of organic aerosols, *Atmos. Chem. Phys.*, 2016, **16**, 3327–3344.

34 N. M. Donahue, E. R. Trump, J. R. Pierce and I. Riipinen, Theoretical constraints on pure vapor-pressure driven condensation of organics to ultrafine particles: ORGANIC CONDENSATION, *Geophysical Research Letters*, 2011, **38**, n/a-n/a.

35 W.-S. W. DeRieux, Y. Li, P. Lin, J. Laskin, A. Laskin, A. K. Bertram, S. A. Nizkorodov and M. Shiraiwa, Predicting the glass transition temperature and viscosity of secondary organic material using molecular composition, *Atmos. Chem. Phys.*, 2018, **18**, 6331–6351.

36 Agency for Toxic Substances and Disease Registry, *Toxicological Profile for Ethylbenzene*, U.S. Department of Health and Human Services, 2010.

37 Comet Chemical Company LTD., *Benzyl alcohol*, 2016.

38 Sigma Aldrich, *Hydroquinone*, Sigma Aldrich, 2023.

39 Toronto Research Chemicals Inc., *2-propenylbenzene*, Toronto Research Chemicals Inc., 2015.

40 Aurochemicals, *Phenyl Ethyl Alcohol*, Aurochemicals, 2019.

41 ThermoFisher Scientific, *4-tert-butyl cyclohexanone*, ThermoFisher Scientific, 2021.

42 Sigma Aldrich, *Divinylbenzene*, Sigma Aldrich, 2022.

43 Sigma Aldrich, *tert-butyl benzene*, Sigma Aldrich, 2022.

44 Sigma Aldrich, *3,3,5-Trimethyl cyclohexanone*, Sigma Aldrich, 2021.

45 *Phthalic Anhydride*, Environmental Protection Agency, 2000.

46 Sigma Aldrich, *Phenanthrene*, Sigma Aldrich, 2023.

47 Sigma Aldrich, *Ethyl benzoylacetate*, Sigma Aldrich, 2022.

48 Sigma Aldrich, *Ethylene glycol dimethacrylate*, Sigma Aldrich, 2019.

49 Sigma Aldrich, *4-tert-butylcyclohexyl acrylate*, Sigma Aldrich, 2019.

50 Sigma Aldrich, *N-butylbenzenesulfonamide*, Sigma Aldrich, 2022.

51 Arkema, *Tert-butyl 2-ethylhexaneperoxoate*, Arkema, 2013.

52 Agency for Toxic Substances and Disease Registry, *Toxicological Profile for diethyl phthalate*, U.S. Department of Health and Human Services, 1995.

53 Environmental Protection Agency, *Dibutyl phthalate*, Environmental Protection Agency, 2000.

54 Parchem, *Butyl Benzyl Phthalate*, Parchem, 2009.

55 Sigma Aldrich, *Bisphenol A diglycidyl ether*, Sigma Aldrich, 2022.

56 State of California, *Di(2-ethylhexyl)phthalate (DEHP)*, State of California, California, 2023.

57 Sigma Aldrich, *Dioctyl Phthalate*, Sigma Aldrich, 2023.